Journal of Materials Chemistry A

Accepted Manuscript

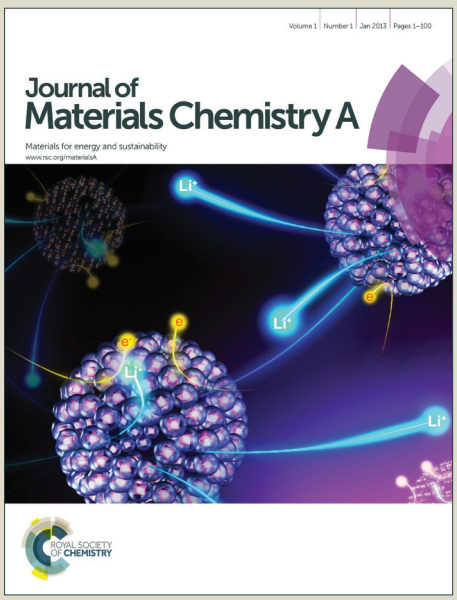

ROYAL SOCIETY OF CHEMISTRY

www.rsc.org/materialsA

Cite this: DOI: 10.1039/c0xx00000x

www.rsc.org/xxxxxx

ARTICLE TYPE

Heteropoly acid and ZrO_2 bifunctionalized organosilica hollow nanospheres for esterification and transesterification

Fang Su, Sai An, Daiyu Song, Xianghuan Zhang, Bo Lu, Yihang Guo*[a]

Received (in XXX, XXX) Xth XXXXXXXXX 20XX, Accepted Xth XXXXXXXXX 20XX

DOI: 10.1039/b000000x

Single-micelle-templated preparation of heteropoly acid and ZrO_2 bifunctionalized organosilica hollow nanospheres ($H_3PW_{12}O_{40}/ZrO_2$-*Et*-HNS) is developed by co-hydrolysis and -condensation of bissilylated organic precursor, 1,2-bis(trimethoxysilyl)ethane (BTMSE), with zirconium source ($Zr(OC_4H_9)_4$) in the presence of $H_3PW_{12}O_{40}$, triblock copolymer surfactant F127 and 1,3,5-trimethylbenzene (TMB) followed by boiling ethanol washing. Through tuning the molar ratios of Si/Zr in the initial gel mixture, the morphology transformation from 3D interconnected mesostructure to the hollow spherical nanostructure is realized. The inner diameter of the $H_3PW_{12}O_{40}/ZrO_2$-*Et*-HNS materials is in the range of 6–12 nm, and their shell thickness is *ca.* 2 nm. As the novel organic-inorganic hybrid catalysts, the catalytic activity of $H_3PW_{12}O_{40}/ZrO_2$-*Et*-HNS is evaluated by the model reactions of esterification of levulinic acid (LA) with methanol to methyl levulinate and transesterification of yellow horn oil with methanol to biodiesel under refluxing temperature (65 ^oC) and atmospheric pressure. The obtained excellent heterogeneous acid catalytic activity of $H_3PW_{12}O_{40}/ZrO_2$-*Et*-HNS is explained in terms of their strong Brönsted and Lewis acidity, unique hollow nanospherical morphology and hydrophobic surface. Finally, the recyclability of the hybrid catalysts is tested through three consecutive catalytic runs.

1 Introduction

Rational design of catalysts with unique morphological characteristics and perfect textural properties has been the long term research focus in the field of catalysis. To a great extent, the catalytic activity of catalysts is determined by their morphological characteristics and textural properties in addition to the chemical structure and composition, which can influence the active site numbers, the accessibility of active sites on a given catalyst surface and inside the pores to the substrates as well as mass-transport of the reactant or product molecules.[1–5] Recently, fabrication of catalysts with various nanostructures, such as nanospheres, nanowires, nanotubes, nanorods and nanopores has been reported.[6–10] Among them, hollow nanospheres catalysts with outstanding properties including hollow interiors, permeable and thin shells, low density, thermal and mechanical stability as well as bimodal mesoporosity have attracted particular interests, and they can serve as the novel nanoreactors for various chemical transformations.[11–13] Generally, various active species could be incorporated into both the hollow interior and the shell of silica, organosilica or carbon hollow nanospheres, however, compared with the preparation of pure silica, organosilica or carbon hollow nanospheres, the fabrication of silica-, organosilica- or carbon-based hollow nanospheres composites/hybrids functionalized by various catalytically active components *via* one-pot route rather than post-synthesis grafting method is more difficult, and only a limited number of research papers is concerned about this topic.[14–16] Therefore, the preparation route should be designed carefully to ensure the structural integrity of the functionalities and perfect hollow nanospherical morphology with controllable particle size. The general approaches for the fabrication of hollow nanospheres composites/hybrids include soft/hard template and self-templating methods depending on the nature of the template.[17] For example, the assembly of silicate or organosilicate species and the active precursors around the template (*e.g.* surfactant micelles and PS spheres) through a sol-gel process and the subsequent removal of templates results in the formation of silica- or organosilica-based hollow nanospheres composite/hybrid catalysts. A successful example has recently been reported by Yang's group. They prepared a series of Pd-doped propylsulfonic acid-functionalized hollow nanospheres (Pd/SO_3H-E-HS) by co-condensation of 1,2-bis(trimethoxysilyl)ethane (BTMSE) with 3-mercaptopropyltrimethoxysilane (MPTMS) in the presence of single surfactant (F127, $EO_{106}PO_{70}EO_{106}$) and salting-out inorganic electrolyte (NaOAc) followed by H_2O_2 postsynthesis oxidation, and subsequent impregnation of metallic Pd. As-prepared Pd/SO_3H-E-HS exhibited a higher activity than their bulk mesoporous counterparts (*e.g.* Pd/SO_3H-SBA-15 and Pd/SO_3H-FDU-12) in the one-pot synthesis of methyl isobutyl ketone (MIBK) from acetone and hydrogen in liquid phase.[18]

Motivated by the aforementioned work, herein, both Keggin-type heteropoly acid and ZrO_2 functionalized ethane-bridged organosilica hollow nanospheres hybrid materials ($H_3PW_{12}O_{40}/ZrO_2$-*Et*-HNS) are successfully fabricated *via* the

carefully designed single step sol-gel route. The preparation procedures include one-step co-condensation of BTMSE and $Zr(OC_4H_9)_4$ around the F127 polymer micelles in the presence of 1,3,5-trimethylbenzene (TMB) and $H_3PW_{12}O_{40}$ and subsequent removal of the polymer. By the combination of unique morphological characters such as spheres with hollow interiors, extremely small particle size and thin shell thickness with Brönsted and Lewis acidity,[19–21] as-prepared $H_3PW_{12}O_{40}/ZrO_2$-*Et*-HNS organic-inorganic hybrid materials are expected to be promising heterogeneous acid catalysts in various important acid-catalyzed reactions.

In the $H_3PW_{12}O_{40}/ZrO_2$-*Et*-HNS hybrid catalysts, $H_3PW_{12}O_{40}$ is an important super strong Brönsted acid that has exhibited excellent catalytic behaviors in a wide variety of acid-catalyzed reactions, and the disadvantages of $H_3PW_{12}O_{40}$ including small specific surface area and high solubility in polar media can be overcome by dispersing it within various porous materials.[22–25] Additionally, selecting ZrO_2 (rather than catalytically inert silica) as the support is due to its both Brönsted and Lewis acidity,[26,27] and the Brönsted acidity of the Keggin units is further enhanced due to strong W–O–Zr covalent bindings between $H_3PW_{12}O_{40}$ clusters and ZrO_2 support, which can promote the release of the protons.[28,29] Meanwhile, the strong interaction between $H_3PW_{12}O_{40}$ and ZrO_2 can effectively inhibit the leakage of $H_3PW_{12}O_{40}$ that generally occurred in most of the supported heteropolyacids, leading to $H_3PW_{12}O_{40}/ZrO_2$-*Et*-HNS a genuine heterogeneous acid catalyst that will find out important applications. Therefore, ZrO_2 can act both acidic site and support in the as-prepared hybrid catalysts. Finally, with ethyl groups bridged in the silica/carbon framework of the prepared $H_3PW_{12}O_{40}/ZrO_2$-*Et*-HNS, the porosity and surface hydrophobicity/hydrophilicity balance of the hybrid catalyst can be tuned dramatically by changing the initial molar ratios of Si to Zr, which can also influence the catalytic behaviors of the catalyst.

To evaluate the heterogeneous acid catalytic performance of as-prepared $H_3PW_{12}O_{40}/ZrO_2$-*Et*-HNS hybrid catalyst, the following two model reactions are selected under refluxing temperature (65 ^oC) and atmospheric pressure: i) synthesis of methyl levulinate from biomass-derived platform molecule, levulinic acid (LA). Methyl levulinate is a member of levulinate ester family that is versatile chemical feedstocks with numerous potential applications in the flavoring and fragrance industry or as a blending component in biodiesel;[30–32] and ii) transesterification of yellow horn (a kind of inedible plant) oil with methanol to produce biodiesel. Biodiesel is a mixture of C_{12}–C_{22} fatty acid monoalkyl esters (FAMEs), and it is a sustainable, sulfur-free, biodegradable and non-toxic fossil fuel substitute that is widely used worldwide. Conventional catalysts for both of the reactions are inorganic liquid acids like HCl and H_2SO_4. Although these liquid acids are efficient to the above processes, they suffer from serious contamination and corrosion problems that make essential the implementation of good separation and purification steps. A "*green*" approach to levulinate esters and biodiesel synthesis has stimulated the application of sustainable solid acid catalysts as replacements for such liquid acid catalysts so that the use of harmful substances and generation of toxic wastes are avoided; meanwhile, the ease of catalyst separation after the reactions can be realized. The catalytic activity of the $H_3PW_{12}O_{40}/ZrO_2$-*Et*-HNS is also compared with the reference acid catalysts including previously reported 2D hexagonal *p6mm* $H_3PW_{12}O_{40}/ZrO_2$-*Et*-$2D_{hex}$,[19] bridging ethyl group-free $H_3PW_{12}O_{40}/ZrO_2$,[33] $H_3PW_{12}O_{40}$, $Cs_{2.5}H_{0.5}PW_{12}O_{40}$, ZrO_2 and commercially available sulfonic ion-exchange resin (Amberlyst-15) under the same conditions. Based on the catalytic testing results, the influence of Brönsted acid-site density, morphological and textural properties as well as surface hydrophobicity on the heterogeneous acid catalytic activity of as-prepared hybrid catalysts is revealed. Finally, the recyclability of the hybrid catalysts is tested through three consecutive catalytic runs.

2 Experimental

2.1 Materials

$H_3PW_{12}O_{40}\bullet xH_2O$, Pluronic F127 ($EO_{106}PO_{70}EO_{106}$, where EO = $–CH_2CH_2O–$, PO = $–CH_2(CH_3)CHO–$, M_w = 12600), Pluronic P123 ($EO_{20}PO_{70}EO_{20}$, M_w = 5800), 1,2-bis(trimethoxysilyl)ethane (BTMSE, 97%), zirconium *n*-butoxide ($Zr(OC_4H_9)_4$, 76–80 % in *n*-butanol) and levulinic acid (LA, 98 %) are purchased from Sigma–Aldrich; methyl levulinate (> 99.0 %) was purchased from TCI. Yellow horn oil is commercially available. The above reagents are used without further purification.

2.2 Catalytic preparation

Preparation of $H_3PW_{12}O_{40}/ZrO_2$-Et-HNS hybrid catalysts. To investigate the effect of molar ratios of precursors (*i.e.* $Zr(OC_4H_9)_4$ and BTMSE) on the morphology of the products, various initial Si/Zr molar ratios (*i.e.* 0.5, 1.0, 1.5 and 2.0) were employed to synthesis the hybrid catalysts while keeping the total molar number of precursors constant (5 mmol). The detailed synthesis route is as follow. F127 (0.5 g) and TMB (2.3 mL) were dissolved in an HCl solution (2 mol L^{-1}, 29 mL). The solution was stirred at 40 ^oC for 3 h. Subsequently, to the above solution, BTMSE (0.25–0.63 mL), $Zr(OC_4H_9)_4$ (1.8–1.1 mL) and aqueous $H_3PW_{12}O_{40}$ (0.110–0.112 g in 1.0 mL water) was added dropwise at hourly interval. The resultant mixture was stirred at 40 ^oC for 24 h and aged at 100 ^oC for another 24 h. Finally, the surfactant-free white precipitate was harvested through air-dried at 100 ^oC overnight, washed three time with boiling ethanol and then air-dried at 100 ^oC for another 12 h. The product is denoted as $H_3PW_{12}O_{40}/ZrO_2$-*Et*-HNS*n*, where *n* is the molar ratio of Si/Zr. For comparison, $H_3PW_{12}O_{40}$-*Et*-HNS was prepared *via* the above process except that BTMSE (5 mmol, 1.27 mL) was used as the only precursor.

Preparation of $H_3PW_{12}O_{40}/ZrO_2$-Et-$2D_{hex}$2.0. P123 (0.275 g) was dissolved in a mixture of water (8.5 mL) and HCl (12 mol L^{-1}, 0.6 mL) under vigorous stirring at room temperature. Subsequently, BTMSE (0.42 mL), $Zr(OC_4H_9)_4$ (0.75 mL) and aqueous $H_3PW_{12}O_{40}$ (0.074 g in 1.5 mL water) were added dropwise to the above solution at hourly intervals, successively. The resulting mixture was stirred at 40 ^oC for 24 h, and then it was transferred into the autoclave and put it into the oven. The temperature of oven was heated up to 120 ^oC at a heating rate of 2 ^oC min^{-1} and then held for 24 h at 120 ^oC. The resulting white solid powder was air-dried at 100 ^oC overnight, and then P123 in the product was removed by boiling ethanol washing.

2.3 Catalyst characterization

TEM observations were performed on a JEM-2100F high resolution transmission electron microscope at an accelerating voltage of 200 kV. Nitrogen gas porosimetry measurement was performed on a Micromeritics ASAP 2020M surface area and porosity analyzer after the samples were outgassed under vacuum at 363 K for 1 h and 373 K for 4 h. The surface areas were calculated using the Brunauer-Emmett-Teller (BET) equation, while pore size distribution curves were calculated using Barrett-Joyner-Halenda (BJH) adsorption branch of the isotherms, and the pore volume was accumulated up to $P/P_0 = 0.99$. ^{31}P MAS NMR, ^{13}C CP-MAS NMR and ^{29}Si MAS NMR spectra were recorded on a Bruker AVANCE III 400 WB spectrometer equipped with a 4 mm standard bore CP MAS probe head. The dried and finely powdered samples were packed in the ZrO_2 rotor closed with Ke–F cap which were spun at 12 KHz rate. Chemical shifts for all ^{31}P MAS NMR, ^{13}C CP-MAS NMR and ^{29}Si MAS NMR spectra were referenced to the signal of $NH_4H_2PO_4$ standard (δ = 0.00), $C_{10}H_{16}$ standard (δCH_2 = 38.5) and 3-(trimethylsilyl)-1-propanesulfonic acid sodium salt standard (δ = 0.0), respectively. FTIR spectra were recorded on a Nicolet Magna 560 IR spectrophotometer. Thermogravimetric analysis (TGA) was performed with a Shimadzu TG instrument at a heating rate of 10 ^oC min^{-1} in air.

2.4 Determination of Brönsted acid-site density

The Brönsted acid-site density of as-prepared materials was determined by acid-base titration. Fresh catalyst powder (60 mg) was placed in 15 mL deionized water, and the mixture was sealed and stirred at 30 ^oC for 24 h. The obtained suspension was cooled down to room temperature, and then it was titrated by sodium hydroxide solution (0.0045 mol L^{-1}) that has been titrated with a standard potassium hydrogen phthalate solution (0.005 mol L^{-1}). The Brönsted acid-site density could be calculated from the consumed sodium hydroxide amount, and it is expressed by the number of equivalents of H^+ ($A_{titration}$, μeq g^{-1}).[34]

2.5 Characterization of Brönsted and Lewis acidity

Brönsted and Lewis acidity of the catalysts was characterized by *in situ* FTIR spectroscopy with chemical adsorption of pyridine. The catalyst samples were mixed with KBr powder and pre-treated at 100 ^oC for 12 h in vacuum. The samples were then exposed to pyridine vapour at 60 ^oC for 12 h in vacuum, followed by pumping out at 150 ^oC for 1 h to remove the physisorbed pyridine. Then, the FTIR spectra of adsorbed pyridine were recorded.

2.6 Catalytic tests

The catalysts were dried for 2 h at 120 ^oC in vacuum before the catalytic tests. All the reactions were carried out in a three-necked round bottomed glass flask fitted with a water cooled condenser. For esterification of LA with methanol, a mixture that consisted of LA (1.474 g or 12.7 mmol), methanol (3.7 mL or 91.5 mmol) and catalyst (88 mg or 2 wt.%) was heated to 65 ^oC for 2 h at atmospheric pressure. For transesterification of yellow horn oil with methanol, the mixture that was composed of yellow horn oil (1.023 g or 1.1 mmol), methanol (4 mL or 98.9 mmol) and catalyst (209 mg or 5 wt%) was heated to 65 ^oC for 24 h at atmospheric pressure. The reaction progress was monitored by taking a small portion (0.1 mL) of the reaction mixture at a specified time. The solid catalysts were removed by centrifugalization, and the obtained liquid was diluted with acetone to 5 mL in order to analyze by GC (Shimadzu 2014C, coupled with a flame ion detector and an HP-INNOWAX capillary column (film thickness, 0.5 μm; *i.d.*, 0.32 mm; length, 30 m), the operation temperature was 220 ^oC and flow rate of nitrogen gas was 1.0 mL/min).

For esterification reaction, ethyl laurate was applied as the internal standard, and the catalytic activity was evaluated quantitatively by the yield of methyl levulinate (Y, %) and turnover frequency (TOF, h^{-1}). Herein, Y (%) = (M_D/M_T) × 100, where M_D and M_T is the number of moles of methyl levulinate produced and expected, respectively; TOF (h^{-1}) = [$M_D/(A_{titration} \times m)$] × t^{-1}, where $A_{titration}$ is the number of equivalents of H^+ determined by acid-base titration (see section 2.4), m (g) is the mass of hybrid catalyst used in the esterification reaction, and t (h) is the reaction time.

For transesterification reaction, ethyl laurate was applied as the internal standard, and the catalytic activity was evaluated quantitatively by the yield of each FAME (Y, %). Herein, Y (%) = (M_D/M_T) × 100, where M_D and M_T are the number of moles of FAME produced and expected, respectively. The FAMEs produced in the reaction system were identified by a mass spectrometry coupled with gas chromatography (HP6890GC-5973MSD) analysis. The GC-MS was equipped with HP-5MS capillary column (film thickness, 0.25 μm; *i.d.*, 0.2 mm; length, 30 m) and helium as the carrier gas at 1 mL min^{-1}. The temperature program was as follows: 150 °C for 2 min, 5 °C/min up to 250 °C, hold time of 10 min. The GC injector and MS ion source temperatures were 250 °C and 230 °C, respectively. The MS detector was operated in the EI mode at 70 eV with a scanning range of m/z 20-500. The concentrations of FAMEs were determined by GC.

3 Results and discussion

3.1 Preparation and characterization of $H_3PW_{12}O_{40}/ZrO_2$-*Et*-HNS organic-inorganic hybrid catalysts

$H_3PW_{12}O_{40}/ZrO_2$-*Et*-HNS hybrid catalysts are prepared by a single step sol-gel route, and the procedures include co-hydrolysis and -condensation of bissilylated organic precursor (BTMSE) with zirconium source ($Zr(OC_4H_9)_4$) in the presence of $H_3PW_{12}O_{40}$, triblock copolymer surfactant F127 and TMB. The procedures of preparation of $H_3PW_{12}O_{40}/ZrO_2$-*Et*-HNS are complicated due to poor processability of heteropoly acid clusters. Moreover, the circumstance is more difficult especially including non-silica component (*i.e.* ZrO_2) in the hybrid materials because the hydrolysis rate of the zirconium precursors is faster in comparison of silicon precursors. $H_3PW_{12}O_{40}$ begins to decompose at pH higher than 1.5 and loses all acidic protons at 465 ^oC.[35,36] Therefore, creating $H_3PW_{12}O_{40}/ZrO_2$-*Et*-HNS should avoid decomposition of the Keggin unit. As a consequence, acidity of the preparation system should be controlled at pH lower than 1.5 and boiling ethanol washing rather than high temperature calcination is selected to remove various additives (*e.g.* F127 and TMB). In addition, the heteropolyanions can

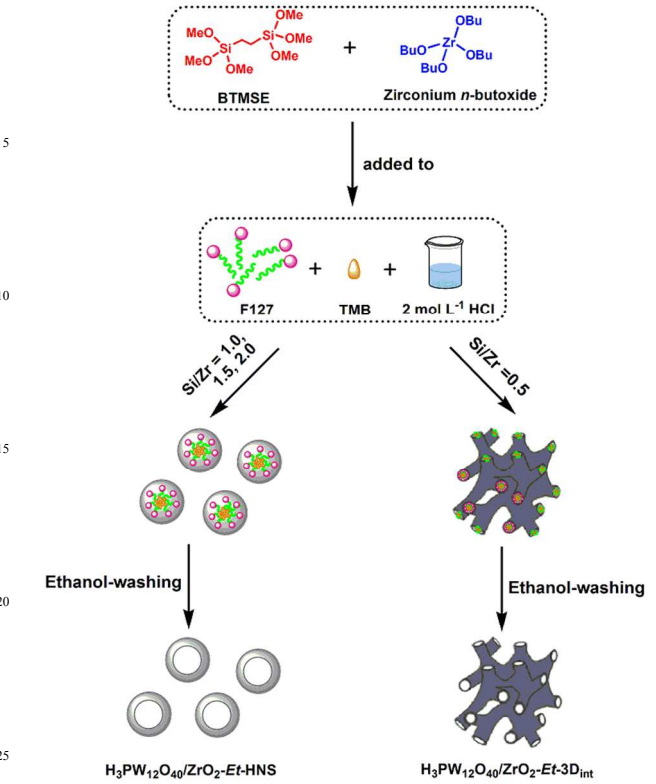

Scheme 1 The representative procedure for the preparation of $H_3PW_{12}O_{40}/ZrO_2$-*Et* hybrid catalysts.

perturb the self-assembly of BTMSE, $Zr(OC_4H_9)_4$ and F127A micelles due to their strong complexation with non-ionic surfactants.[37] Therefore, the preparation conditions should be controlled carefully to create a suitable environment for self-assembling BTMSE and $Zr(OC_4H_9)_4$ around F127 micelles, which is the key step to fabrication of $H_3PW_{12}O_{40}/ZrO_2$-*Et*-HNS.

At the beginning of preparation of organic-inorganic hybrid hollow nanospheres materials, the single surfactant (F127) micelles are formed by copolymer assembly *via* hydrogen bonding and hydrophobic/hydrophilic interactions in a dilute HCl solution (2mol L^{-1}) with the assistance of TMB. That is, hydrophobic PPO blocks form a core of the micelle, while hydrophilic PEO blocks form a hydrated corona around the core. These F127 micelles are served as soft templates for constructing $H_3PW_{12}O_{40}/ZrO_2$-*Et*-HNS. Subsequently, co-hydrolysis and -condensation of BTMSE with $Zr(OC_4H_9)_4$ in the presence of $H_3PW_{12}O_{40}$ leads to $H_3PW_{12}O_{40}/Zr(OC_4H_9)_{4-x}(OH_2^+)_x$–$Si(OSi)_n(OH)_{3-n}$–$C_2H_4$–$Si(OSi)_n(OH)_{3-n}$ (x = 1–4, n = 1–3) species. It should be mentioned that the hydrolysis rate of BTMSE is obviously slower than that of $Zr(OC_4H_9)_4$. In order to ensure the matching of hydrolysis rate between BTMSE and $Zr(OC_4H_9)_4$, prehydrolysis of BTMSE at 40 °C for 1 h is proceeded before the addition of $Zr(OC_4H_9)_4$ and $H_3PW_{12}O_{40}$. The assembly of the hydrolyzed species around the corona of individual F127 micelles results in the formation of spherical supramolecular complexes $H_3PW_{12}O_{40}/Zr(OC_4H_9)_{4-x}(OH_2^+)_x$–$Si(OSi)_n(OH)_{3-n}$–$C_2H_4$–$Si(OSi)_n(OH)_{3-n}$–$EO_{106}PO_{70}EO_{106}$. After further aging and subsequent boiling ethanol washing for F127 removing, $H_3PW_{12}O_{40}/ZrO_2$–$Si(OSi)_3$–C_2H_4–$Si(OSi)_3$ (abbreviated as $H_3PW_{12}O_{40}/ZrO_2$-*Et*) organic-inorganic hybrid hollow spheres are formed. It has been reported that the single surfactant micelles formed by copolymer (*e.g.* F127 or P123) assembly in an aqueous solution are usually in the meso-scale (2–50 nm).[17] Therefore, F127 single micelles-templated $H_3PW_{12}O_{40}/ZrO_2$-*Et* hollow spheres are expected to be in the particle size less than 100 nm; additionally, in the presence of TMB, the charge density on the surface of F127 micelles was further decreased due to the penetration of hydrophobic TMB into the micelles, which may lead to dispersed single micelles and thus finally to the well-dispersed hollow nanospheres. Based on the above discussion, schematic illustration of the formation of $H_3PW_{12}O_{40}/ZrO_2$-*Et*-HNS hybrid materials is presented in Scheme 1.

Pore morphologies and textural properties. TEM technique is an effective measurement method to reveal the morphology change of the nanomaterials. The representative TEM images of the $H_3PW_{12}O_{40}/ZrO_2$-*Et* organic-inorganic hybrid materials prepared at different initial Si/Zr molar ratios (*e.g.* 0.5, 1.0, 1.5 and 2.0) are collected in Fig. 1. At Si/Zr molar ratio of 0.5, the material (*e.g.* $H_3PW_{12}O_{40}/ZrO_2$-*Et*-$3D_{int}$) mainly exhibits 3D interconnected mesostructure, and only a small quantity of sphere-like hollow particles is observed (highlighted with arrow, Fig. 1a). As for the materials prepared at Si/Zr molar ratio of 1.0, 1.5 and 2.0 (*e.g.* $H_3PW_{12}O_{40}/ZrO_2$-*Et*-HNS*1.0*, $H_3PW_{12}O_{40}/ZrO_2$-*Et*-HNS*1.5* and $H_3PW_{12}O_{40}/ZrO_2$-*Et*-HNS*2.0*), they mainly exhibit hollow spherical morphologies with the inner diameter in the range of 6–12 nm (or particle size of 10–16 nm) and shell thickness of *ca.* 2 nm (Fig. 1b-d). In the case of ZrO_2-free $H_3PW_{12}O_{40}$-*Et*-HNS obtained by the same route, its hollow spherical nanostructre becomes perfect with the inner diameter of *ca.* 12 nm (or particle size of 18 nm) and shell thickness of *ca.* 3 nm (Fig. 1e). As expected, 2D hexagonal *p6mm* mesostructure of $H_3PW_{12}O_{40}/ZrO_2$-*Et*-$2D_{hex}$*2.0* (obtained by one step P123-directed sol-gel–hydrothermal process) can be clearly observed in Fig. 1f. The above results suggest that initial Si/Zr molar ratios in the preparation systems influence the morphology formation of $H_3PW_{12}O_{40}/ZrO_2$-*Et* organic-inorganic hybrid materials obviously. On the one hand, the morphology of the hybrid materials is related to the hydrophobicity/hydrophilicity of the precursors (*e.g.* BTMSE and $Zr(OC_4H_9)_4$). Generally, BTMSE is a hydrophobic silicate precursor due to the existence of organic groups (*i.e.* ethyl), while $Zr(OC_4H_9)_4$ is a hydrophilic precursor compared with BTMSE. Formation of F127 single spherical micelles can be encouraged by the hydrophobic unhydrolyzed BTMSE since the charge density on the surface of F127 micelles is decreased owing to the penetration of the hydrophobic unhydrolyzed BTMSE into the micelles. The hydrophobicity/hydrophilicity of the preparation system tends to more hydrophobic with the increased initial Si/Zr molar ratio, as a result, the morphology transformation from 3D interconnected mesostructure to the hollow spherical nanostructure occurs.[38] On the other hand, hydrolysis/condensation rate of BTMSE and $Zr(OC_4H_9)_4$ influences the morphology of the resulting hybrid materials. The precursor with faster hydrolysis/condensation rate (*e.g.* $Zr(OC_4H_9)_4$) can produce more hydrolyzed species (*e.g.* $Zr(OC_4H_9)_{4-x}(OH_2^+)_x$) to condense around the single micelles, which in turn results in the aggregation of F127 single micelles. Accordingly, the hybrid materials with the bulk mesostructure are

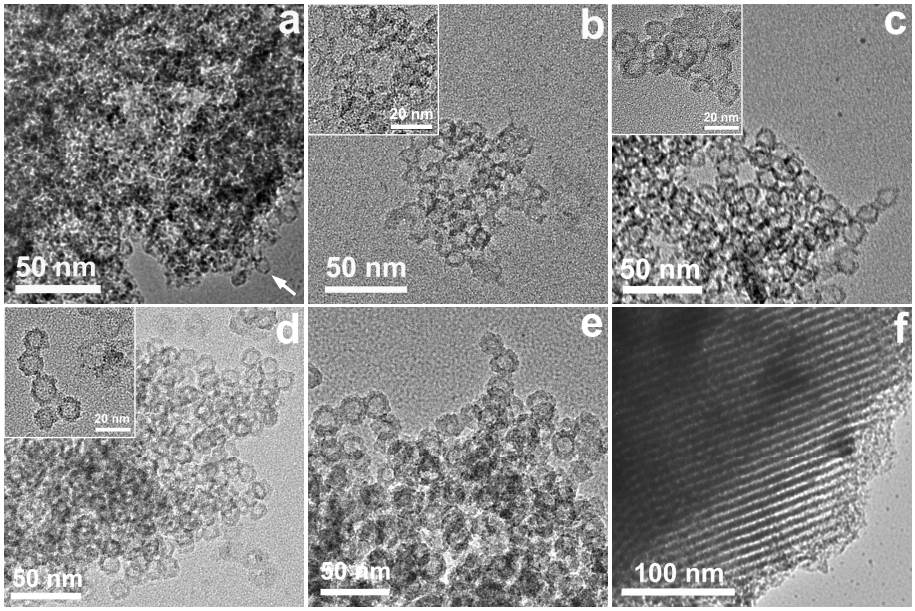

Fig. 1 The representative TEM images of as-prepared hybrid catalysts. $H_3PW_{12}O_{40}/ZrO_2$-*Et*-3D$_{int}$ (a); $H_3PW_{12}O_{40}/ZrO_2$-*Et*-HSN*1.0* (b); $H_3PW_{12}O_{40}/ZrO_2$-*Et*-HSN*1.5* (c); $H_3PW_{12}O_{40}/ZrO_2$-*Et*-HSN*2.0* (d); $H_3PW_{12}O_{40}$-*Et*-HSN (e) and $H_3PW_{12}O_{40}/ZrO_2$-*Et*-2D$_{hex}$*2.0* (f).

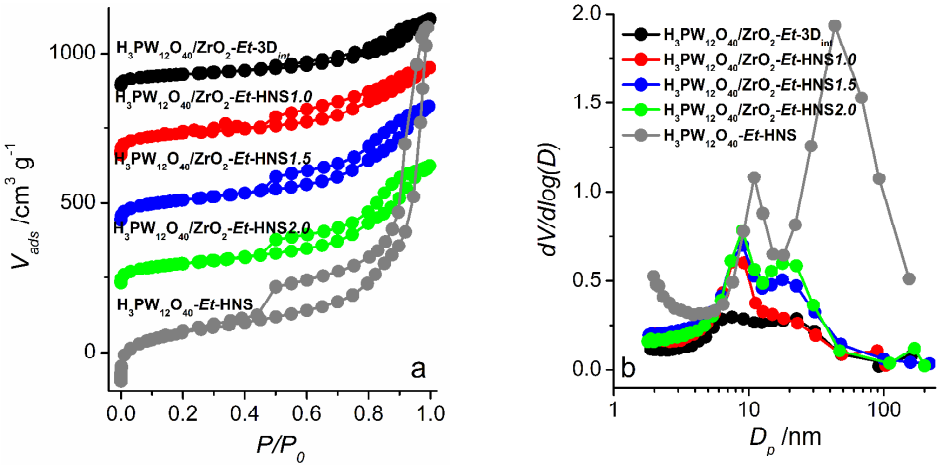

Fig. 2 Nitrogen gas adsorption-desorption isotherm (a) and pore size distribution curves (b) of various hybrid catalysts.

obtained. Otherwise, the hydrolysis/condensation rate of BTMSE is much slower, and increasing initial Si/Zr molar ratio can slow down the hydrolysis/condensation rate of the precursors. Therefore, the aggregation of F127 single micelles is inhibited effectively, leading to $H_3PW_{12}O_{40}/ZrO_2$-*Et* hybrid materials with hollow nanospheres structure. Therefore, it is concluded that changing the initial Si/Zr molar ratios in the preparation systems can adjust the hydrophobicity/hydrophilicity and hydrolysis/condensation rate of the precursors, which in turn leads to the morphology transformation of the $H_3PW_{12}O_{40}/ZrO_2$-*Et* hybrid materials from the bulk mesostructure to hollow spherical nanosturctue.

The porosity and textural properties of as-synthesized materials are characterized by nitrogen gas physisorption analysis. Nitrogen gas adsorption-desorption isotherms and pore size distribution curves of various $H_3PW_{12}O_{40}/ZrO_2$-*Et* hybrid materials as well as $H_3PW_{12}O_{40}$-*Et*-HNS are present in the Fig. 2. From Fig. 2a it is found that all tested hybrid materials exhibit type IV isotherm, implying their mesoporosity. In addition, rapidly increased nitrogen gas adsorbed amount at low relative pressure regions (P/P_0 < 0.1) suggests that as-prepared hybrid materials also have microporosity. The microporosity originates from the more hydrophilic EO chains of the surfactant, which penetrate the wall during synthesis and lead to microporosity.[38] For $H_3PW_{12}O_{40}/ZrO_2$-*Et*-3D$_{int}$ material, it has one capillary condensation step at the relative pressure P/P_0 = 0.40–0.80. In the cases of $H_3PW_{12}O_{40}/ZrO_2$-*Et*-HNS*1.0*, $H_3PW_{12}O_{40}/ZrO_2$-*Et*-HNS*1.5*, $H_3PW_{12}O_{40}/ZrO_2$-*Et*-HNS*2.0* and $H_3PW_{12}O_{40}$-*Et*-HNS, they possess two capillary condensation steps at a relative pressure P/P_0 = 0.40–0.80 and P/P_0 = 0.80–0.99 (close to the saturation vapour pressure), respectively. Combination of the textural properties with morphological characteristics of

Table 1 Textural parameters and Brönsted acid-site density of various hybrid catalysts[a]

Sample	S_{BET}/cm^2 g^{-1}	V_p/cm^3 g^{-1}	D_p/nm	$A_{titration}$/μeq g^{-1}
$H_3PW_{12}O_{40}/ZrO_2$-*Et*-3D$_{int}$	151	0.32	7.5/22.6	2891
$H_3PW_{12}O_{40}/ZrO_2$-*Et*-HSN*1.0*	256	0.43	7.6/17.0	1902
$H_3PW_{12}O_{40}/ZrO_2$-*Et*-HSN*1.5*	265	0.57	9.0/17.7	1833
$H_3PW_{12}O_{40}/ZrO_2$-*Et*-HSN*2.0* 1st[b]	339	0.71	9.1/18.0	1500
$H_3PW_{12}O_{40}$-*Et*-HSN	603	1.34	11.0/43.4	333
$H_3PW_{12}O_{40}/ZrO_2$-*Et*-HSN*2.0* 3rd[c]	313	0.64	9.1/18.0	1200
$H_3PW_{12}O_{40}/ZrO_2$-*Et*-2D$_{hex}$*2.0*	353	0.44	6.4	1327

[a] Pore diameter (D_p) was estimated from BJH adsorption determination; Pore volume (V_p) was estimated from the pore volume determination using the adsorption branch of the N_2 isotherm curve at $P/P_0 = 0.99$ single point; Acid capacity ($A_{titration}$) of the tested catalysts was measured by titration with NaOH (0.0045 mol L^{-1}) and expressed by the number of equivalents of H^+ in the catalysts. [b] The first use of the catalyst in the reaction. [c] The third time of the catalyst was used in the reaction.

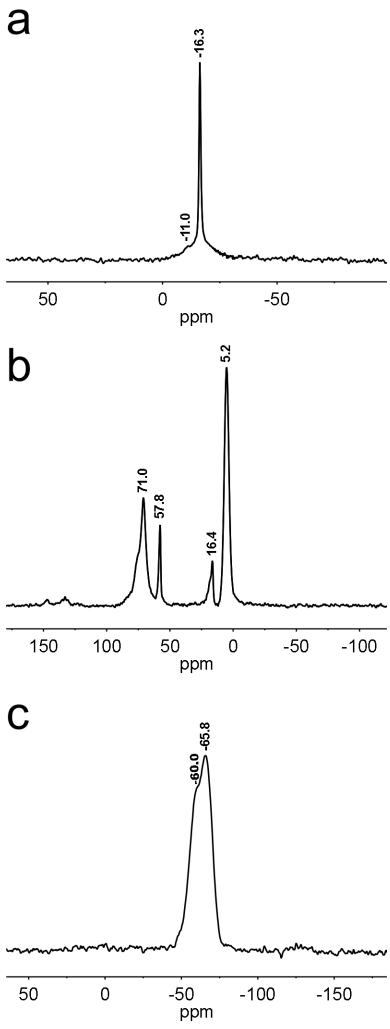

Fig. 3 ^{31}P MAS (a), ^{13}C CP-MAS (b) and ^{29}Si MAS (c) NMR spectra of the as-prepared $H_3PW_{12}O_{40}/ZrO_2$-*Et*-HNS*2.0* hybrid catalyst.

$H_3PW_{12}O_{40}/ZrO_2$-*Et*-HNS hybrid materials it is speculated that the hysteresis loop appeared at a lower relative pressure can be assigned to the hollow interior of the spherical particles; and that the other hysteresis loop shown up at a higher relative pressure originates from void space between the loosely packed spherical particles. Therefore, as-prepared $H_3PW_{12}O_{40}$-*Et*-HNS hybrid materials possess an interesting hierarchical porous structure.

The above results are consistent with BJH pore-size distribution curves displayed in Fig. 2b as well as the textual parameters summarized in Table 1. From Table 1 it is found that: i) the diameter of the primary and secondary pore calculated from BJH adsorption determination is in the range of 7.6–11.0 nm and 17.0–43.4 nm, respectively, for $H_3PW_{12}O_{40}/ZrO_2$-*Et* and $H_3PW_{12}O_{40}$-*Et*-HNS hybrid materials with various morphologies; ii) with the increase of the initial Si/Zr molar ratio, the BET surface area (from 151 to 339 cm^2 g^{-1}), pore diameter (from 7.5/22.6 to 9.1/18.0 nm) and pore volume (from 0.32 to 0.71 cm^3 g^{-1}) of the hybrid materials increase gradually; and iii) among all tested hybrid materials, ZrO_2-free $H_3PW_{12}O_{40}$-*Et*-HNS exhibits the largest BET surface area (603 cm^2 g^{-1}), the largest pore diameter (11.0 nm) and highest pore volume (1.34 cm^3 g^{-1}).

Composition and structure. The loading of $H_3PW_{12}O_{40}$ in all products is 10.0–11.0 wt% except for $H_3PW_{12}O_{40}$-*Et*-HNS (5.7 wt%), determined by a Leeman Prodigy Spec ICP-AES.

The structural integrity of the Keggin units and ethane-bridged organosilica fragments as well as the interaction between the ZrO_2 with organic or inorganic functionalities in the hybrid organic-inorganic hollow nanospheres materials are provided by ^{31}P MAS NMR (Fig. 3a), ^{13}C CP-MAS NMR (Fig. 3b) and ^{29}Si MAS NMR (Fig. 3c) spectra, and $H_3PW_{12}O_{40}/ZrO_2$-*Et*-HNS*2.0* is selected as the representative.

The ^{31}P MAS NMR spectrum of $H_3PW_{12}O_{40}/ZrO_2$-*Et*-HNS*2.0* shows that the strong resonance at –16.3 ppm, which is assigned to the PO_4 units within the bulk $H_3PW_{12}O_{40}$ environment, suggesting the structural integrity of the Keggin units after formation of the organic-inorganic hybrid hollow nanoshperes.

As for the weak signal at −11.0 ppm, it is due to the new $(\equiv ZrOH_2^+)_n[H_{3-n}PW_{12}O_{40}]^{n-}$ species generated at the interface of the Keggin units and ZrO_2.[39] In this species, the terminal W=O bonds of Keggin units can coordinate with the surface ≡ZrOH groups of ZrO_2 *via* Zr–O–W covalent bonds. The conclusion is reasonable because of the well-matched electronegativity and ionic radius of Zr^{4+} ion (1.33, 0.072 nm) and W^{6+} (1.70, 0.060 nm).[31] The interactions ensure strong combination of the Keggin units and ZrO_2 in the organic-inorganic hybrid hollow nanospheres.

In the ^{13}C CP-MAS NMR spectrum of $H_3PW_{12}O_{40}/ZrO_2$-*Et*-HNS*2.0*, a predominant peak at 5.2 ppm originates from the carbon species of ethane-bridged organosilica unit (–Si–CH_2–CH_2–Si–), suggesting that ethane-bridged organosilica units are successfully incorporated into the framework of $H_3PW_{12}O_{40}/ZrO_2$-*Et*-HNS material through –Zr–O–Si–CH_2–CH_2–Si–O– linkages. In the cases of three weak signals at 71.0, 57.8 and 16.4 ppm, they are due to residual F127 and the carbon species of the ethoxy group that are formed during boiling ethanol washing process.[19]

In the ^{29}Si MAS NMR spectrum of $H_3PW_{12}O_{40}/ZrO_2$-*Et*-HNS*2.0*, the characteristic resonances at −60.0 and −65.8 ppm correspond to the organosiloxane species of –CH_2CH_2–$Si(OSi)_2(OH)$ (T^2) and –CH_2CH_2–$Si(OSi)_3$ (T^3) within the ethane-bridged organosilica groups, respectively. The result confirms full framework linkage of ethane-bridged organosilica groups in the shell of the hybrid material.[7] Additionally, the absence of any resonance signal assignable to SiO_4 species such as Q^3 [$Si(OSi)_3(OH)$, −90 ppm] and Q^4 [$Si(OSi)_4$, −120 ppm] confirms that cleavage of the Si–C bond of Si–CH_2CH_2–Si moiety in the silica/carbon framework of $H_3PW_{12}O_{40}/ZrO_2$-*Et*-HNS*2.0* has been avoided.

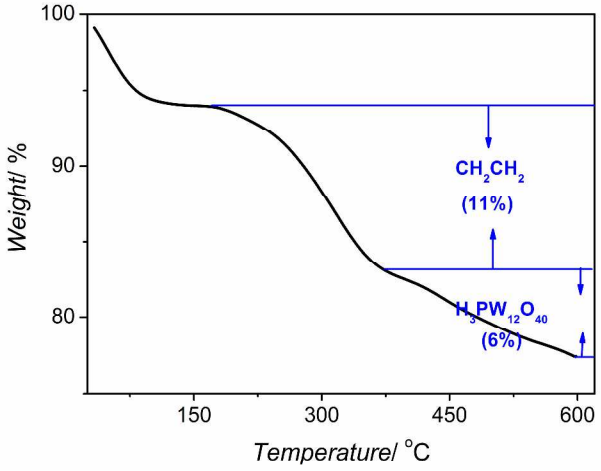

Fig. 4 TGA profile of as-prepared $H_3PW_{12}O_{40}$-*Et*-HNS*2.0* hybrid material.

TGA is conducted in the range of 25–600 °C, and the TGA plot of $H_3PW_{12}O_{40}/ZrO_2$-*Et*-HNS*2.0* is depicted in Fig. 4. The TGA profile shows three weight loss steps: the first weight loss (*ca.* 6%) that occurred below 100 °C is related to the loss of physisorbed water at the hybrid material surface. A main weight loss (*ca.* 11%) in the range of 170–365 °C is assigned to the decomposition of ethane-bridged group.[40] Although the residual surfactants are also decomposition in the same range, it is very difficult to quantify the amount of surfactant.[26] The third weight loss (*ca.* 6%) in the range of 365–600 °C is due to partial decomposition of $H_3PW_{12}O_{40}$.[41] The TGA analysis indicates as-prepared $H_3PW_{12}O_{40}/ZrO_2$-*Et*-HNS is thermal stable at temperature lower than 170 °C.

Based on the above chemical structure information, the illustration of the shell structure and composition of the $H_3PW_{12}O_{40}/ZrO_2$-*Et*-HNS is proposed and illustrated in Scheme 2.

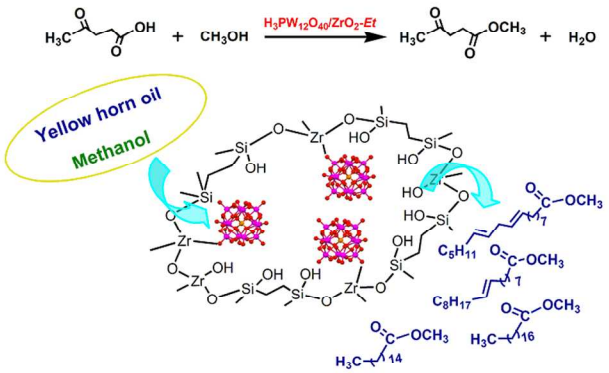

Scheme 2 The shell composition of $H_3PW_{12}O_{40}/ZrO_2$-*Et* hollow nanospheres as well as the processes of levulinic acid esterification and yellow horn oil transesterification catalyzed over $H_3PW_{12}O_{40}/ZrO_2$-*Et* hollow nanospheres hybrid catalysts.

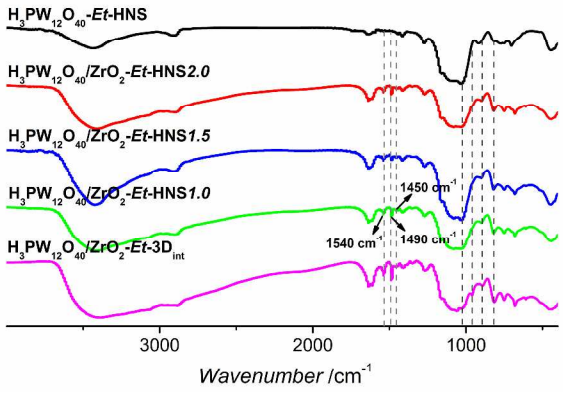

Fig. 5 FTIR spectra of pyridine adsorbed on various as-prepared hybrid catalysts.

Brönsted acid-site density. The Brönsted acid-site density of the $H_3PW_{12}O_{40}/ZrO_2$-*Et* hybrid materials is measured through acid-base titration with NaOH (0.0045 mol L^{-1}). From the acid values summarized in Table 1 it is found that the acid-site density of the tested materials decreases gradually with increasing the initial Si/Zr molar ratio from 0.5, 1.0, 1.5 to 2.0. The finding is owing to the fact that the proportion of the non-acidic silica increases and goes parallel with the initial Si/Zr molar ratio from 0.5 to 2.0. As for ZrO_2-free $H_3PW_{12}O_{40}$-*Et*-HNS, it has the lowest acid capacity (333 μeq g^{-1}).

Brönsted and Lewis acidity. Pyridine-FTIR spectra of various $H_3PW_{12}O_{40}/ZrO_2$-*Et* and $H_3PW_{12}O_{40}$-*Et*-HNS materials are provided to investigate the different types of acid sites in as-prepared hybrid materials (Fig. 5). Three characteristic peaks at 1450, 1490 and 1540 cm^{-1} are observed for four tested $H_3PW_{12}O_{40}/ZrO_2$-*Et* materials. The peak at 1450 cm^{-1} is assigned to the Lewis acid sites, which is due to pyridine coordinatively bond to the unsaturated surface Zr^{4+}. As for the peak at 1540 cm^{-1}, it is related to pyridinium ions formed due to the protonation of

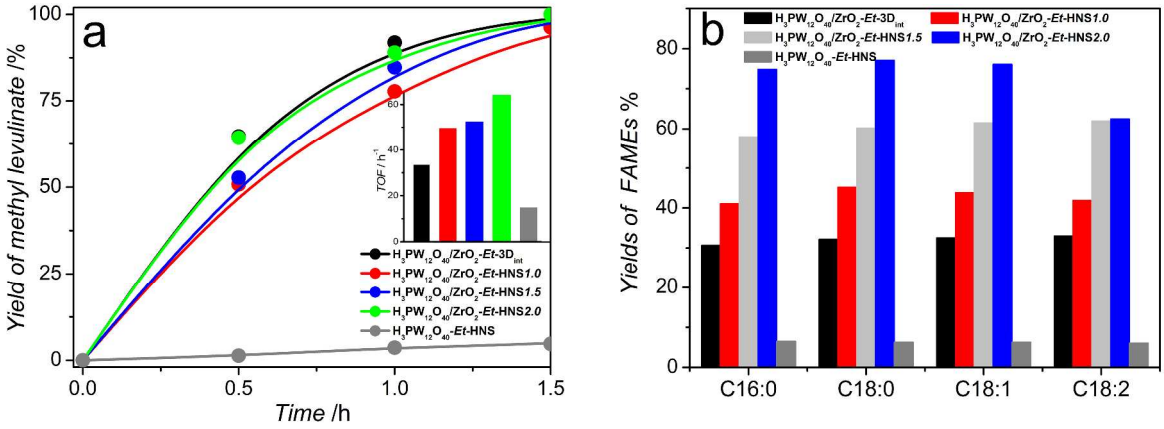

Fig. 6 Catalytic activity of as-prepared catalysts towards esterification of levulnic acid with methanol (a) and transesterification of yellow horn oil with methanol (b). Conditions: molar ratio of LA: methanol = 1: 7, 2 wt% catalyst, 65 °C, 1.5 h, atmospheric pressure (esterification); oil: 1.023 g (1.1 mmol), methanol: 4 mL (98.9 mmol), 5 wt% catalyst, 65 °C, 24 h, atmospheric pressure (transesterification).

the Brönsted acid sites. These Brönsted acid sites are contributed from the protons of $H_3PW_{12}O_{40}$ and surface Zr–OH groups of ZrO_2. The co-existence of Brönsted and Lewis acid sites is confirmed by the characteristic peak at 1490 cm^{-1}. The above results indicate that the $H_3PW_{12}O_{40}/ZrO_2$-*Et* hybrid materials possess both Brönsted and Lewis acid sites, regardless of their morphological characteristic. In the case of $H_3PW_{12}O_{40}$-*Et*-HNS, it only exhibits Brönsted acidity since no peak related to Lewis acid sites or co-existence of Brönsted and Lewis acid sites are found in the $H_3PW_{12}O_{40}$-*Et*-HNS-pyridine-FTIR spectrum.

3.2 Evaluation of heterogeneous acid catalytic performance of $H_3PW_{12}O_{40}/ZrO_2$-*Et* organic-inorganic hybrid catalysts

Catalytic activity. $H_3PW_{12}O_{40}/ZrO_2$-*Et*-HNS organic-inorganic hybrid catalysts with advantages of strong Brönsted and Lewis acidity, hollow nanosphere morphology as well as surface hydrophobicity are expected to exhibit the excellent catalytic performance in heterogeneous acid-catalyzed reactions. In current work, the heterogeneous acid catalytic performance of $H_3PW_{12}O_{40}/ZrO_2$-*Et*-HNS is evaluated by esterification of LA with methanol to synthesize methyl levulinate and transesterification of yellow horn oil with methanol to produce biodiesel (Scheme 2). Both of the reactions need Brönsted and Lewis acid sites; moreover, Lewis acid sites are more active in promoting transesterification reactions.[42]

Firstly, the heterogeneous acid catalytic activity of the $H_3PW_{12}O_{40}/ZrO_2$-*Et* materials prepared at various initial Si/Zr molar ratios are evaluated in the esterification of LA with methanol under the conditions of a 1: 7 molar ratio of LA to methanol, 2 wt% catalyst, 65 °C and atmospheric pressure. From the result presented in Fig. 6a it is found that four tested $H_3PW_{12}O_{40}/ZrO_2$-*Et* materials show excellent esterification activity, and their catalytic activity follows the order $H_3PW_{12}O_{40}/ZrO_2$-*Et*-HNS*1.0* < $H_3PW_{12}O_{40}/ZrO_2$-*Et*-HNS*1.5* < $H_3PW_{12}O_{40}/ZrO_2$-*Et*-HNS*2.0* ≈ $H_3PW_{12}O_{40}/ZrO_2$-*Et*-3D_{int}. For example, the yield of methyl levulinate reaches 78, 85, 89 and 92% after the reaction proceeded for 1 h. As for ZrO_2-free $H_3PW_{12}O_{40}$-*Et*-HNS, it shows the lowest yield of methyl levulinate (3.6%) under the same conditions. In order to compare the catalytic activity in terms of per acid site, TOF (h^{-1}) of each catalyst are given in the inset of Fig. 6a. This result indicates that the catalytic activity of $H_3PW_{12}O_{40}/ZrO_2$-*Et* increases gradually with the increased initial Si/Zr molar ratio; additionally, $H_3PW_{12}O_{40}$-*Et*-HNS*2.0* is the most active among the five tested hybrid catalysts.

To expand the scope of their application, the heterogeneous acid catalytic activity of as-prepared $H_3PW_{12}O_{40}/ZrO_2$-*Et* catalysts is further tested in transesterification of yellow horn oil with methanol to produce biodiesel under the conditions of methanol to oil molar ratio of 90: 1, 5 wt% catalyst, 65 °C and atmospheric pressure. Low price and high yield of this feedstock lead to the biodiesel-production process from inedible yellow horn oil is practical and economical. Thereby, biodiesel-derived from yellow horn oil is expected to be competitive with petroleum-based diesel for the commercial use.

In the $H_3PW_{12}O_{40}/ZrO_2$-*Et*-catalyzed transesterification system, the transesterification products (*i.e.* FAMEs) are identified by a GC-MS. The main FAMEs produced are methyl palmitate (MP, C16:0), methyl stearate (MS, C18:0), methyl oleate (MO, C18:1) and methyl lioleate (ML, C18:2); additionally, a small quantity of methyl eicosenoate (ME, C20:1) and methyl docosenate (MD, C22:0) are also found. Herein, the transesterification acivity of as-prepared three $H_3PW_{12}O_{40}/ZrO_2$-*Et*-HNS hybrid catalysts is evaluated by the yields of four main FAMEs (*i.e.* MP, MS, MO and ML). For comparison, $H_3PW_{12}O_{40}/ZrO_2$-*Et*-3D_{int} and ZrO_2-free $H_3PW_{12}O_{40}$-*Et*-HNS are also tested under the same conditions. From the result displayed in Fig. 6b it is found that the transesterification reaction proceeds more slowly in comparison of esterification reaction. This result is explained by the following three reasons: i) transesterification of triglycerides (TGs) in oily feedstocks is a more complex process with multiple steps; ii) transesterification of TGs can produce more intermediates; and iii) transesterification of TGs needs higher activation energy.[21] From Fig. 6b it is also found that the hybrid catalysts follow the activity order $H_3PW_{12}O_{40}$-*Et*-HNS < $H_3PW_{12}O_{40}/ZrO_2$-*Et*-3D_{int} < $H_3PW_{12}O_{40}/ZrO_2$-*Et*-HNS*1.0* < $H_3PW_{12}O_{40}/ZrO_2$-*Et*-HNS*1.5* < $H_3PW_{12}O_{40}/ZrO_2$-*Et*-HNS*2.0*. For the most active $H_3PW_{12}O_{40}/ZrO_2$-*Et*-HNS*2.0*-catalyzed

transesterification reaction, the yields of MP, MS, MO and ML reach 75, 77, 76 and 63%, respectively, after the reaction proceeded for 24 h.

Compared with the results shown in Fig. 6a and b it is found that the reaction activity of the tested hybrid catalysts (expressed in terms of the yield) towards esterification and transesterification follow the different sequences. For transesterification reaction, mass transfer of TG molecules in yellow horn oil is the rate controlling step because TGs are bulky and high viscosity compounds. The disordered bulk mesostructure with poor porosity (*e.g.* smaller BET surface area, lower pore volume and smaller pore diameter) of the $H_3PW_{12}O_{40}/ZrO_2$-*Et*-3D$_{int}$ leads to the increased mass transfer limit of bulky TG molecules and inaccessible to the acid sites in transesterification process, and thereby, $H_3PW_{12}O_{40}/ZrO_2$-*Et*-3D$_{int}$ exhibits obviously lower transesterification activity compared with $H_3PW_{12}O_{40}$-*Et*-HNS*2.0*. In the case of $H_3PW_{12}O_{40}/ZrO_2$-*Et*-3D$_{int}$-catalyzed esterification process, higher catalytic activity of $H_3PW_{12}O_{40}/ZrO_2$-*Et*-3D$_{int}$ may due to its very high Brönsted acid-site density (2891 μeq g^{-1}), which plays a dominating role in its esterificaiton activity.

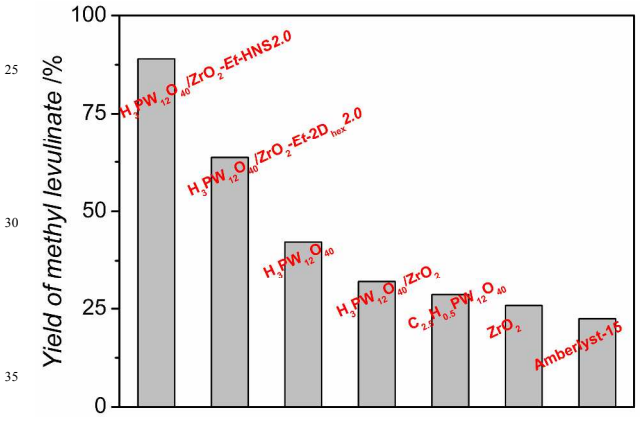

Fig. 7 Comparison of the catalytic activity of $H_3PW_{12}O_{40}/ZrO_2$-*Et*-HNS*2.0* with $H_3PW_{12}O_{40}/ZrO_2$-*Et*-2D$_{hex}$*2.0*, $H_3PW_{12}O_{40}/ZrO_2$, ZrO_2, $C_{2.5}H_{0.5}PW_{12}O_{40}$, pure $H_3PW_{12}O_{40}$ and Amberlyst-15 towards esterification of levulnic acid with methanol. Conditions: molar ratio of LA: methanol = 1: 7, 2 wt% catalyst, 65 °C, 1 h, atmospheric pressure.

Subsequently, the heterogeneous acid catalytic activity of the most active $H_3PW_{12}O_{40}/ZrO_2$-*Et*-HNS*2.0* is compared with six reference catalysts including $H_3PW_{12}O_{40}/ZrO_2$-*Et*-2D$_{hex}$*2.0*, $H_3PW_{12}O_{40}/ZrO_2$, $H_3PW_{12}O_{40}$, $Cs_{2.5}H_{0.5}PW_{12}O_{40}$, ZrO_2 and Amberlyst-15 by selecting esterification of LA with methanol as the model reaction. From the result displayed in Fig. 7 it is found that the heterogeneous acid catalytic activity of $H_3PW_{12}O_{40}/ZrO_2$-*Et*-HNS*2.0* outperforms all of the tested reference catalysts. For example, the yield of methyl levulinate reaches 89 ($H_3PW_{12}O_{40}/ZrO_2$-*Et*-HNS*2.0*), 64 ($H_3PW_{12}O_{40}/ZrO_2$-*Et*-2D$_{hex}$*2.0*), 42 ($H_3PW_{12}O_4$), 32 ($H_3PW_{12}O_{40}/ZrO_2$), 29 ($Cs_{2.5}H_{0.5}PW_{12}O_4$), 26 ($ZrO_2$), and 22% (Amberlyst-15), respectively, after the reaction performed for 1 h.

Discussion. Based on the physicochemical properties and catalytic testing results of as-prepared $H_3PW_{12}O_{40}/ZrO_2$-*Et*-HNS organic-inorganic hybrid catalysts, their excellent catalytic activity is explained in terms of the strong Brönsted and Lewis acidity, unique hollow nanospherical morphology and hydrophobic surface.

First of all, the inherent strong Brönsted and Lewis acidity plays the dominant role to the excellent catalytic activity of the $H_3PW_{12}O_{40}/ZrO_2$-*Et*-HNS hybrid catalysts. The Brönsted acidity of the hybrid catalysts originates from $H_3PW_{12}O_{40}$ and ZrO_2; moreover, the Brönsted acid strength can be enhanced owing to the formation of $(\equiv ZrOH_2^+)_n[H_{3-n}PW_{12}O_{40}]^{n-}$ species at the interface between $H_3PW_{12}O_{40}$ and ZrO_2.[28,29,43] With the aid of the protons, carbonyl groups of LA or TG molecules are protonated at the beginning of the esterification or transesterification reaction. This is the key step for both of the reactions, and strong Brönsted acidity of the hybrid catalysts can facilitate the reactions proceeding at a fast rate. On the other hand, the Lewis acid sites of the hybrid catalysts come from coordinatively unsaturated Zr^{4+} sites of ZrO_2, which leave the exposed Zr^{4+} ion to interact directly with LA or TG molecules and act as the acceptor of the electron-pair. In the subsequent steps, they follow the same procedures as those of the Brönsted acid-catalyzed esterification or transesterification reaction.

Secondly, unique hollow nanospherical morphology of the $H_3PW_{12}O_{40}/ZrO_2$-*Et*-HNS hybrid catalysts with shell thickness in several nanometers can serve as the nanoreactors where esterification or transesterification reaction takes place. For the $H_3PW_{12}O_{40}/ZrO_2$-*Et*-HNS-catalyzed reactions, the diffusion path of the reactants and products is shortened; moreover, the accessibility of acid sites to the reactants could be increased. Both of the factors can speed up the mass transport of the reactants and/or products, which results in the enhancement of the esterification and transesterification activity.[17,18] Additionally, unique hollow nanospherical structure of $H_3PW_{12}O_{40}/ZrO_2$-*Et*-HNS led to them excellent textural properties including hierarchical porous structure, larger BET surface area (256–339 m^2 g^{-1}) and high pore volume (0.43–0.71 cm^3 g^{-1}), which can provide better dispersion of the acid sites throughout the hybrid catalysts and increase the population of the acid sites. Accordingly, the accessibility of LA or TGs molecules to the acid sites also could be increased, giving a positive influence on the catalytic activity. For the tested three hollow nanospherical hybrid catalysts, $H_3PW_{12}O_{40}/ZrO_2$-*Et*-HNS*1.0*, $H_3PW_{12}O_{40}/ZrO_2$-*Et*-HNS*1.5* and $H_3PW_{12}O_{40}/ZrO_2$-*Et*-HNS*2.0*, their BET surface area, pore diameter and pore volume increase with Si/Zr molar ratio. Accordingly, $H_3PW_{12}O_{40}/ZrO_2$-*Et*-HNS*1.0* and $H_3PW_{12}O_{40}/ZrO_2$-*Et*-HNS*2.0* exhibit the lowest and highest esterification or transesterification activity. In the case of $H_3PW_{12}O_{40}/ZrO_2$-*Et*-2D$_{hex}$*2.0*, although it has the similar textural properties to those of $H_3PW_{12}O_{40}/ZrO_2$-*Et*-HNS*2.0*, its lower catalytic activity with respect to its hollow sphere-like counterpart is due to the lengthened diffusion pathway (pore channels of bulk mesoporous counterpart is longer). However, for ZrO_2-free $H_3PW_{12}O_{40}$-*Et*-HNS, although it has perfect hollow nanospherical structure and excellent porosity characteristic (BET surface area 603 m^2 g^{-1}; pore volume 1.34 cm^2 g^{-1}), it exhibits the lowest esterification and transesterification activity among all tested hybrid catalysts. This is due to its low acidity because it only has the Brönsted acid sites. Therefore, it is inferred that the catalytic activity of as-prepared hybrid catalysts is closely related

to their morphological properties in addition to the chemical structure and composition.

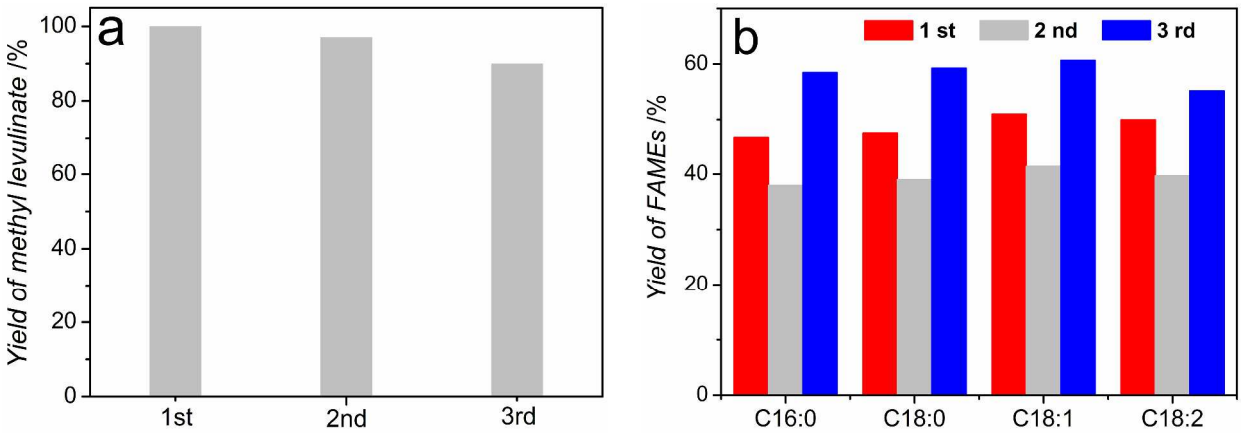

Fig. 8 Reusability of $H_3PW_{12}O_{40}/ZrO_2$-*Et*-HNS*2.0* hybrid catalyst towards the esterfication of levulnic acid with methanol (a) and transesterification of yellow horn oil with methanol (b). Conditions: molar ratio of LA: methanol = 1: 7, 2 wt% catalyst, 65 °C, 2 h, atmospheric pressure (esterification); oil: 1.023 g (1.1 mmol), methanol: 4 mL (98.9 mmol), 5 wt% catalyst, 65 °C, 12 h, atmospheric pressure (transesterification).

Finally, hydrophobic surface of the hybrid catalysts owing to incorporation of bridging ethyl groups in the framework is also responsible for the excellent esterification and transesterification activity. The hydrophobic environment in the pore channels is in favor of enrichment of hydrophobic reactants (*i.e.* LA or TG), while the hydrophilic products like water or glycerol are expelled. Accordingly, the esterification of LA and transesterification of yellow horn oil can proceed at a fast rate. At the same time, the catalyst deactivation due to the strong interaction of the active site with water or glycerol is dramatically reduced, which is confirmed by the following recycling test (Fig. 8).

3.3 Regeneration and reusability

The stability of the active sites and the reusability of the heterogeneous catalysts in the liquid reaction system have been of concern for the hybrid/composite catalysts. Therefore, the most active $H_3PW_{12}O_{40}/ZrO_2$-*Et*-HNS*2.0* catalyst is selected to study the stability and reusability of as-prepared heterogeneous catalysts. The processes are performed three times, and the results are shown in Fig. 8. After the first use and before every subsequent reuse, the catalyst is recovered by centrifugation, washed three times with dichloromethane and dried at 100 °C in air. The new reaction begins with refilling new reactants and the weighed reused catalyst under the optimum reaction conditions, *i.e.* molar ratio of LA to methanol is 1: 7, 2 wt% catalyst, 65 °C, 2 h and atmospheric pressure for LA esterification; molar ratio of methanol to oil is 90 to 1, 5 wt% catalyst, 65 °C, 12 h and atmospheric pressure for yellow horn oil transesterification. From the results displayed in Fig. 8 it is found that the catalytic activity of $H_3PW_{12}O_{40}/ZrO_2$-*Et*-HNS*2.0* is almost retained after three cycles for LA esterification (Fig. 8a) and yellow horn oil transesterification reaction (Fig. 8b).

Additionally, P and W in the catalyst-free reaction solutions are not detected by ICP-AES; meanwhile, changes of structural properties and acidity of the reused hybrid catalyst are negligible (entry 6 in Table 1). Therefore, the loss of activity during the recycling process may be owing to the loss of the catalyst powder. The result indicates that $H_3PW_{12}O_{40}/ZrO_2$-*Et*-HNS*2.0* hybrid catalyst is a recyclable and water-tolerant solid catalyst for the LA esterification and yellow horn oil transesterification. The high catalytic stability is attributed to: i) the strong chemical interaction between the Keggin units and ZrO_2; and ii) the hydrophobic catalyst surface, which can inhibit the strong adsorption of water or glycerol effectively.

4 Conclusions

A series of heteropoly acid and ZrO_2 bifunctionalized organosilica hollow nanospheres ($H_3PW_{12}O_{40}/ZrO_2$-*Et*-HNS) hybrid catalysts are successfully fabricated by carefully designed sol-gel co-condensation route. By the combination of advantageous including strong Brönsted and Lewis acidity, unique hollow nanospherical morphology and hydrophobic surface, as-prepared organic-inorganic hybrid catalysts exhibit excellent heterogeneous acid catalytic activity in the synthesis of methyl levulinate from levulinic acid and biodiesel production from yellow horn oil under mild conditions. The inherent Brönsted and Lewis acidity of the hybrid catalysts facilitate both of the esterifiation and transesterification reactions carrying out at a fast rate; additionally, the unique hollow nanospherical morphology of the hybrid catalysts with thin shell thickness and unique textural properties including bimodal porous structure with hollow interior and interparticle voids, larger BET surface area and high pore volume can increase the accessibility of the guest molecules to the acid sites, reduce the diffusion resistance, shorten the diffusion pathway, provide better dispersion of the acid sites throughout the hybrid catalysts and increase the population of the acid sites; and finally, the hydrophobic surface of the hybrid catalysts is in favor of hydrophobic reactants enrichment as well as expels the hydrophilic products, which also can speed up both of the reactions. The strong interaction between the Keggin unit and ZrO_2 effectively inhibit the leakage of the acid sites, and thereby the hybrid catalysts can be reused at least three times without significant activity loss.

Acknowledgements

This work was supported by the Natural Science Fund Council of China (21173036; 51278092).

Notes and references

[a] *School of Chemistry, Northeast Normal University, Changchun 130024, P.R. China. Tel./fax: +86 431 85098705. E-mail: guoyh@nenu.edu.cn (Y. Guo)*

† Electronic Supplementary Information (ESI) available: [details of any supplementary information available should be included here]. See DOI:10.1039/b000000x/

‡ Footnotes should appear here. These might include comments relevant to but not central to the matter under discussion, limited experimental and spectral data, and crystallographic data.

1 J. Dhainaut, J. P. Dacquin, A. F. Lee and K. Wilson, *Green Chem.*, 2010, **12**, 296–303.
2 J. Du, X. Y. Lai, N. L. Yang, J. Zhai, D. Kisailus, F. B. Su, D. Wang and L. Jiang, *ACS Nano*, 2011, **5**, 590–596.
3 C. C. Li, J. Dou, L. W. Chen, J. Y. Lin and H. C. Zeng, *ChemCatChem*, 2012, **4**, 1675–1682.
4 L. Qin, X. X. Pan, L. Wang, X. P. Sun, G. L. Zhang and X. W. Guo, *Appl. Catal. B: Environ.*, 2014, **150–151**, 544–553.
5 X. Zhang, H. X. Chen, Y. P. Xie and J. X. Guo, *J. Mater. Chem. A*, 2014, **2**, 3912–3918.
6 D. H. Niu, Z. J. Liu, Y. S. Li, X. F. Luo, J. Y. Zhang, J. P. Gong and J. L. Shi, *Adv. Mater.*, DOI: 10.1002/adma.201400815.
7 M. Mandal and M. Kruk, *Chem. Mater.*, 2012, **24**, 123–132.
8 P. S. Archana, A. Gupta, M. M. Yusoff and R. Jose, *Phys. Chem. Chem. Phys.*, 2014, **16**, 7448–1454.
9 O. Al-Youbi, J.L. G. de la Fuente, F.J. Pérez-Alonso, A. Y. Obaid, J.L.G. Fierro, M.A. Pena, M. A. Salam and S. Rojas, *Appl. Catal. B: Environ.*, 2014, **150–151**, 21–29.
10 J. P. Lai, L. Zhang, W. X. Niu, W. J. Qi, J. M. Zhao, Z. Y. Liu, W. Zheng and G. B. Xu, *Nanotechnology*, 2014, **25**, 125601 (1–5).
11 Y. Yang, X. Liu, X. B. Li, J. Zhao, S. Y. Bai, J. Liu and Q. H. Yang, *Agew. Chem.*, 2012, **124**, 9298–9302.
12 S. Y. Bai, J. Liu, J. S. Gao, Q. H. Yang and C. Li, *Micropor. Mesopor. Mater.*, 2012, **151**, 474–480.
13 N. Hao, H. T. Wang, P. A. Webley and D. Y. Zhao, *Micropor. Mesopor. Mater.*, 2010, **132**, 543–551.
14 R. Liu, R. H. Jin, J. Z. An, Q. K. Zhao, T. Y. Cheng and G. H. Liu, *Chem. Asian. J.*, 2014, DOI: 10.1002/asia.201301543.
15 H. C. Xin, J. Zhao, X. B. Li, J. T. Tang, Q. H. Yang, *Micropor. Mesopor. Mater.*, 2014, **190**, 54–62.
16 X. W. Wu and C. M. Crudden, *Chem. Mater.*, 2012, **24**, 3839–3846.
17 X. B. Li, Y. Yang and Q. H. Yang, *J. Mater. Chem. A*, 2013, **1**, 1525–1535.
18 P. Wang, S. Y. Bai, J. Zhao, P. P. Su, Q. H. Yang and C. Li, *ChemSusChem*, 2012, **5**, 2390–2396.
19 F. Su, L. Ma, D. Y. Song, X. H. Zhang and Y. H. Guo, *Green Chem.*, 2013, **15**, 885–890.
20 F. Su, Q. Y. Wu, D. Y. Song, X. H. Zhang, M. Wang and Y. H. Guo, *J. Mater. Chem. A*, 2013, **1**, 13209–13221.
21 F. Su and Y. H. Guo, *Green Chem.*, 2014, **16**, 2934–2957.
22 M. L. Granados, M. D. Zafra Poves, D. M. Alonso, R. Mariscal, F. C. Galisteo, R. Moreno-Tost, J. Santamaría and J. L. G. Fierro, *Appl. Catal. B: Environ.*, 2007, **73**, 317–326.
23 P. Felizardo, M. J. Neiva Correia, I. Raposo, J. F. Mendes, R. Berkemeier and J. M. Bordado, *Waste Manage.*, 2006, **26**, 487–494.
24 M. G. Kulkarni and A. K. Dalai, *Ind. Eng. Chem. Res.*, 2006, **45**, 2901–2913.
25 Y. Wang, S. Ou, P. Liu, F. Xue and S. Tang, *J. Mol. Catal. A: Chem.*, 2006, **252**, 107–112.
26 A. M. Alsalme, P. V. Wiper, Y. Z. Khimyak, E. F. Kozhevnikova and I. V. Kozhevikov, *J. Catal.*, 2010, **276**, 181–189.
27 B. Samaranch, P. R. Piscina, G. Clet, M. Houalla, P. Gélin and N. Homs, *Chem. Mater.*, 2007, **19**, 1445–1451.
28 M. G. Kulkarni, R. Gopinath, L. C. Meher and A. K. Dalai, *Green Chem.*, 2006, **8**, 1056–1062.
29 B. M. Devassy and S. B. Halligudi, *J. Catal.*, 2005, **236**, 313–323.
30 R. I. Khusnutdinov, A. R. Baiguzina, A. A. Smirnov, R. R. Mukminov and U. M. Dzhemilev, *Russ. J. Appl. Chem.*, 2007, **80**, 1687–1690.
31 D. J. Hayes, S. W. Fitzpatrick, M. H. B. Hayes and J. R. H. Ross, Biorefineries Industrial Process and Product (Eds.: B. Kamm, P. R. Gruber, M. Kamm), Wiley-VCH, Weinheim, 2005, 139–164.
32 H. Oshi, B. R. Moser, J. Toler, W. F. Smith and T. Walker, *Biomass Bioenergy*, 2011, **35**, 3262–3266.
33 F. Su, L. Ma, Y. H. Guo and W. Li, *Catal. Sci. Technol.*, 2012, **2**, 2367–2374.
34 A. A. Kiss, A. C. Dimian and G. Rothenberg, *Adv. Synth. Catal.*, 2006, **348**, 75–81.
35 Y. H. Guo, K. X. Li and J. H. Clark, *Green Chem.*, 2007, **9**, 839–841.
36 Y. H. Guo, K. X. Li, X. D. Yu and J. H. Clark, *Appl. Catal. B: Environ.*, 2008, **81**, 182–191.
37 G. S. Armatas, G. Bilis and M. Louloudi, *J. Mater. Chem.*, 2011, **21**, 2997–3005.
38 J. Liu, S. Y. Bai, H. Zhong, C. Li and Q. H. Yang, *J. Phys. Chem. C*, 2010, **114**, 953–961.
39 T. Okuhara, *Chem. Rev.*, 2002, **102**, 3641–3666.
40 P. Van Der Voort, D. Esquivel, E. De Canck, F. Goethals, I. Van Driessche and F. J. Romero-Salguero, *Chem. Soc. Rev.*, 2013, **42**, 3913–3955.
41 M. A. Wahab, II. Kim and Chang-Sik Ha, *Micropor. Mesopor. Mater.*, 2004, **69**, 19–27.
42 E. Santacesaria, G. M. Vicenteb, M. D. Serioa and R. Tesser, *Catal. Today*, 2012, **195**, 2–13.
43 E. Lopez-Salinas, J. G. Hernandez-Cortez, I. Schifter, E. Torres-Garcia, J. Navarrete, A. Gutierrez-Carrillo, T. Lopez, P. P. Lottici and D. Bersani, *Appl. Catal. A: Gren.*, 2000, **193**, 215–225.

Table of contents entry

Title: Heteropoly acid and ZrO_2 bifunctionalized oraganosilica hollow nanospheres for esterification and transesterification

Authors: Fang Su, Sai An, Daiyu Song, Xianghuan Zhang, Bo Lu, Yihang Guo*[a]

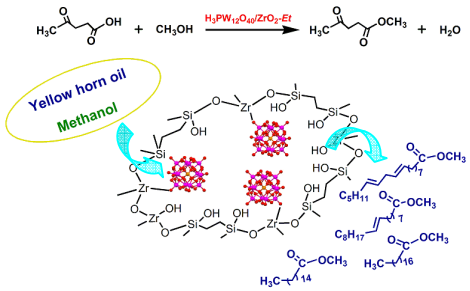

$H_3PW_{12}O_{40}/ZrO_2$-*Et*-HNS materials with strong Brönsted and Lewis acidity, unique hollow nanospherical morphology and enhanced surface hydrophobicity exihibit excellent catalytic activity.